Journal of Theoretical and Applied Mechanics, Sofia, Vol.54 (2024) pp. 186-200
SOLID MECHANICS

WAVE SCATTERING BY NANOINLCUSIONS IN ANISOTROPIC PLANE. PART I: MECHANICAL MODEL

SONIA PARVANOVA[1]*, PETIA DINEVA[2]

[1]*Department of Structural Engineering,*
University of Architecture, Civil Engineering and Geodesy, Sofia, Bulgaria
[2]*Institute of Mechanics, Bulgarian Academy of Sciences, Sofia, Bulgaria*

[Received: 05 April 2023. Accepted: 11 May 2024]

doi: https://doi.org/10.55787/jtams.24.54.2.186

ABSTRACT: Elastic time-harmonic and transient wave scattering by multiple anisotropic nanoiclusions is the object of this study. The nanoinclusions are situated in an infinite anisotropic medium under plane strain conditions. The model is in the frame of surface elasticity theory proposed by Gurtin-Murdoch in 1975 [1]. The computational tool is a combination of the boundary integral equations method (BIEM) based on the frequency dependent elastodynamic fundamental solution for anisotropic continua, Gurtin-Murdoch theory, and Fourier integral transforms. Stress concentration factors and scattered wave displacements for nanoinclusions swept by pressure or shear waves are computed. The benchmark cases used for verification of the developed numerical scheme, illustrate the accuracy of the present methodology. Finally, in the companion paper (Part II), the detailed parametric study is presented and discussed.

KEY WORDS: wave scattering, in-plane wave motion, anisotropic nanoinclusions, infinite anisotropic plane, BIEM, dynamic response in frequency and time domain.

1 INTRODUCTION

The main objective of this paper is to develop a mechanical elastodynamic model at nanoscale and to verify the worked out efficient computational methodology based on the direct boundary integral equation method (BIEM). Elastic wave scattering by a system of anisotropic nanoinclusions in infinite generally anisotropic plane subjected to time-harmonic and transient incident P/SV wave is considered. The application background of multiple nanoinclusions problem can be found in nanomechanics concerning nanocomposite material structures. To the best of our knowledge, the wave scattering by multiple anisotropic nanoinclusions in an infinite anisotropic

*Corresponding author e-mail: slp_fce@uacg.bg

plane under transient wave has not been dealt with yet. A detail review on the mechanical models in nanomechanics can be seen in Manolis et al. [2,3]. The following basic conceptual models are available in the literature: (a) discrete models at atomistic/molecular and mesoscopic level. The '*ab initio*' models are described by the quantum mechanics of electrons and nuclei governed by the Schrödinger equation at length scale $h \approx 10^{-9}$ m. The atomistic models ($h \approx 10^{-7}$ m) are based on Newtonian mechanics, with main components the atoms plus the interaction laws derived from quantum mechanics. The mesoscopic models ($h \approx 10^{-4}$ m) work with the main players clusters of atoms or molecules and lattice defects; (b) Pure continuum mechanics models ($h \approx 10^{-2}$ m), where the field variables (density, temperature, strain, displacement, stress) are all continuous functions. The mechanical state is based on constitutive laws capturing the effects of the microstructure and based on empirical phenomenological rules. The advanced continuum mechanics models aim to extend of the range of classical solid mechanics by bridging its basic theoretical principles with the most fundamental effects observed at the nano level. Such models are: non-local elasticity theory; higher-order strain gradient and higher-order nonlocal strain gradient elasticity theory; surface elasticity models with the Gurtin-Murdoch [1] model being the most common one; (c) multiscale material models, which aim to achieve the balance between the microstructural information complexity and the abstractions in continuum theory.

Speaking about inclusions at macrolevel, dynamic analytical solutions are confined to simple geometries and material models even for elastic isotropic media, see Pao and Mow [4]. The study of wave scattering by macroinclusions of arbitrary shape in isotropic/anisotropic materials requires the use of numerical techniques. The volumetric approaches such as finite difference and finite element methods are completely volume dependent, leading to systems of great number of DOFs. Among the advanced numerical techniques, the mesh-reducing boundary element method (BEM) has been proven as accurate computational tool (see, e.g., the book by Dominguez [5]). It is well-known the BEM is an attractive tool for wave propagation in infinite media due to the following advantages: (a) the integral equation formulation is equivalent to the original governing equation. This fact, coupled with the use of the fundamental solutions of the governing equation, ensures a high level of accuracy; (b) the fundamental solutions obey the Sommerfeld's radiation condition. This means that infinitely extended domains are automatically covered without the usage of special types of viscous boundaries; (c) since only surfaces need to be modelled, there is a reduction of the problem dimensionality; (d) the method is flexible in treating of arbitrary geometry.

Although the well-known advantages of the BEM in solving inclusions problems at the macroscale, their application in nanomechanics is still limited. The problem is

that at the nanoscale ($10^{-7} > h > 10^{-9}$) the continuum approaches begin to break down, while discrete methods reach inherent time and size limitations. In analyzing the mechanical behavior of nanomaterials, a key feature is the intrinsic surface stresses that arise due to their large surface areas. At the atomic scale, the microscopic structure of the surface of a body or of an interface between bodies is quite different from that associated with the interior. This can be described macroscopically by an excess free energy of a surface/ interface and by the corresponding surface/interface stress. The mathematical framework for incorporating surface stresses into continuum mechanics framework was established by Gurtin and Murdoch [1]. Elastodynamic time-harmonic solutions for isotropic nanoinclusions in infinite elastic isotropic media in the frame of surface elasticity model are available in [6–11].

The lack of solutions regarding the in-plane wave motion in generally anisotropic infinite plane containing anisotropic nanoinclusions motivates the authors to focus on this problem. The proposed model is in the frame of the surface elasticity theory, achieved by the boundary integral equations along the contact interfaces between the matrix and nanoinclusions. The proposed BIEM is based on the frequency-dependent fundamental solution of 2D elastodynamics for general anisotropic continuum.

The paper has the following structure: the problem statement and its reformulation via integral equations along the interface boundaries between the matrix and nanoinclusions are presented in Section 2. The accuracy and verification of the numerical scheme is studied in Section 3 and finally, conclusions are discussed in the last Section 4. A detailed parametric simulation is presented in an accompanied paper – Part II of this study.

2 Problem Statement via Boundary Integral Equations

Plane strain state in the plane $\Gamma(x_3 = 0)$ is under consideration. The infinite elastic anisotropic plane Γ containing N elastic anisotropic nanoinclusions $\Omega_{I,k}$ with boundaries $\Gamma_I = \cup_{k=1}^{N} \Gamma_{I,k}$ ($\Gamma_I \in \Gamma$) is subjected to incident time-harmonic or transient longitudinal P or shear SV wave, see Fig. 1. The following notations $c_{ij,I}$, ρ_I and $c_{ij,M}$, ρ_M for stiffness characteristics and density of inclusions and matrix, respectively, are used. The 2D general anisotropy is characterized by six elastic constants c_{11}, c_{12}, c_{16}, c_{22}, c_{26}, c_{66}, which in the case of orthotropic material are reduced to the four ones c_{11}, c_{12}, c_{22}, c_{66}.

The aim is to model in-plane elastic wave motion in a generally anisotropic infinite plane containing multiple anisotropic nanoinclusions with arbitrary number, mutual configuration and geometrical shape. The goal is to calculate numerically the dynamic non-uniform stress-strain distribution, displacements and local stress concentration zones in the nanoheterogeneous plane.

The case of transient wave will be solved by application of direct fast Fourier

transform (FFT) with respect to the time variable and solution of the defined below boundary-value problem (BVP) in frequency domain. The solution in time domain is obtained after application of inverse FFT to the solutions in frequency domain. The BVP in frequency domain is formulated via governing equation (1) and boundary condition (2) along the interface boundaries Γ_I.

$$\sigma_{ij,j}\left(\mathbf{x},\omega\right)+\rho\omega^2 u_i\left(\mathbf{x},\omega\right)=0, \qquad \mathbf{x}\left(x_1,x_2\right)\in\Gamma\,. \tag{1}$$

Here: $\mathbf{x}\left(x_1,x_2\right)$ is the radius-vector of the observer point; σ_{ij} is the stress in the matrix denoted by σ_{ij}^M or the stress $\sigma_{ij}^{I,k}$ of the k-th inclusion; the respective strains ε_{ij} are denoted as ε_{ij}^M or $\varepsilon_{ij}^{I,k}$; u_i being u_i^M or $u_i^{I,k}$ are the corresponding displacements, ω is the angular frequency, density ρ is ρ_I or ρ_M. Comma subscripts denote partial differentiation with respect to the spatial coordinates and the summation convention over repeated indices is assumed.

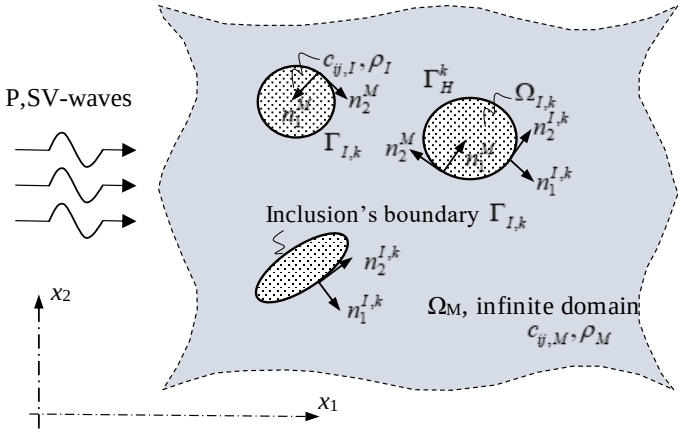

Fig. 1: Problem formulation.

A model compatible with the theory of elastodynamics is the one proposed by Gurtin-Murdoch [1], who established the mathematical framework for incorporating surface stresses into continuum mechanics formulations. This theory was motivated in part by empirical observations pointing to the presence of a compressive surface stress in certain types of crystals. In the Gurtin-Murdoch model, the interfaces between nano-heterogeneities and the bulk matrix are regarded as infinitely thin surfaces that possess their own deformation and surface tension characteristics. A linearized surface stress–strain constitutive relation was proposed to characterize this surface/interface effect. More specifically, the equilibrium and constitutive equations of the bulk solid are the same as those in classical elasticity, but the presence

of a surface/interface stress gives rise to *non-classical boundary conditions*. The surface stress tensor is associated with both the bulk stress tensor and the external load by means of a force balance equation established at the solid's surface. Under the assumption of small deformations, a linear constitutive relationship between surface stress and surface strain is established via a fourth-order tensor comprising the *surface elastic moduli* and the resulting system is mathematically complete. We note that the linearized Gurtin–Murdoch theory has attracted much interest and has been used to explain size-dependent properties of nanostructures and nanocomposites. Important results have been obtained recently in the field of computational mechanics, listed in the review paper by Manolis et al. [2].

It is assumed that the thin interface layer between any nanoinclusion and matrix is with zero thickness, elastic and isotropic, while the bulk solid is elastic and anisotropic. The surface stresses due to the presence of surface effects depend on the corresponding strain along the interface. The detailed expressions could be seen in Parvanova et al. [9]. The Gurtin-Murdoch model is applied to the contact interface as far as its implementation in the model is involved with respect to the interface displacements which are one and the same for the surfaces bonding together.

Non-classical boundary conditions (2), derived by Gurtin-Murdoch [1], which take into account the free energy excess along interfaces Γ_I are satisfied along the total boundary of the nanoinclusions Γ_I:

$$\begin{Bmatrix} t_1^{I,k} + t_1^{M,k} \\ t_2^{I,k} + t_2^{M,k} \end{Bmatrix}_k = -\frac{\tau_0}{\kappa} \begin{Bmatrix} n_1 \\ n_2 \end{Bmatrix} + \mathbf{T}^S \begin{Bmatrix} u_1^k \\ u_2^k \end{Bmatrix}, \tag{2}$$

$$\mathbf{T}^S = \mathbf{T}_1 + \frac{\partial}{\partial l}\mathbf{T}_2 + \frac{\partial^2}{\partial l^2}\mathbf{T}_3\,, \tag{3}$$

$$\mathbf{T_1} = \frac{1}{\kappa^2}\mathbf{N} \begin{bmatrix} -\alpha^S & \tau_0\kappa_{,l} \\ -\alpha^S\kappa_{,l} & -\tau_0 \end{bmatrix} \mathbf{N}^T; \tag{4}$$

$$\mathbf{T_2} = \mathbf{N} \begin{bmatrix} 0 & -\beta \\ \beta & 0 \end{bmatrix} \mathbf{N}^T; \quad \mathbf{T_3} = \mathbf{N} \begin{bmatrix} \tau_0 & 0 \\ 0 & \alpha \end{bmatrix} \mathbf{N}^T,$$

$$\mathbf{N} = \begin{bmatrix} n_1 & -n_2 \\ n_2 & n_1 \end{bmatrix}, \tag{5}$$

where $\alpha^S = \lambda^S + 2\mu^S$ is the surface elasticity modulus, which usually falls into the limits of $\pm 10N/m$, see Tian and Rajapakse [12]; $\beta = (\alpha^S/\kappa + \tau_0/\kappa)$, κ is the curvature radius for the k-th interface boundary $\Gamma_{I,k}$; $n_i = n_i^{I,k} = -n_i^{M,k}$; λ^S, μ^S are the elastic constants of the zeroth thin interface $\Gamma_{I,k}$; deformations along

all the interfaces follow linear elastic isotropic constitutive equation $\sigma_{ll}^S = \tau^0 + (\lambda^S + 2\mu^S)\varepsilon_{ll}^S$, here σ_{ll}^S, ε_{ll}^S are stress and strain in tangential to the surface direction; $\partial/\partial l$ and $\partial^2/\partial l^2$ are the first and second tangential derivatives, respectively; τ_0 is the residual surface tension under unstrained conditions, which induces an additional static deformation only. The residual surface tension τ_0 is often ignored in dynamic analyses. In the specific case of $\alpha^S = 0$ and $\tau_0 = 0$, the above boundary condition (2) transforms into the classical boundary condition describing the tractions continuity along the interfaces.

By the usage of the dynamic Betti's reciprocity theorem and the fundamental solution of the elastodynamic equation for 2D anisotropic material, see Dominguez [5], the above defined problem can be described via boundary integral equations (6) along the interface boundaries Γ_I:

$$C_{ij}u_j^{sc}(\mathbf{x},\omega) = \int_{\Gamma_I} U_{ij}^*(\mathbf{x},\xi,\omega)t_j^{sc}(\xi,\omega)d\Gamma(\xi) - \int_{\Gamma_I} T_{ij}^*(\mathbf{x},\xi,\omega)\, u_j^{sc}(\xi,\omega)d\Gamma(\xi)\,. \tag{6}$$

Here $\mathbf{x} = (x_1, x_2) \in \Gamma_I$; C_{ij} is the jump term depending on the local geometry at the source point $\mathbf{x} = (x_1, x_2)$; the couple $\mathbf{x}, \xi$ presents the position vectors of the source and receiver $\xi = (\xi_1, \xi_2)$ respectively; $U_{ij}^*(\mathbf{x},\xi,\omega)$ is the displacement fundamental solution of the governing elliptic partial differential equation for in-plane wave motion in generally anisotropic solid, and its corresponding traction is $T_{ij}^*(\mathbf{x},\xi,\omega) = C_{ijql}U_{qk,l}^*(\mathbf{x},\xi,\omega)n_k$, see [13, 14].

The boundary integral equation (6) is written for the scattered wave displacement $u_i^{\text{sc}} = u_i - u_i^{\text{inc}}$ and traction $t_i^{\text{sc}} = t_i - t_i^{\text{inc}}$, where u_i and t_i present the total displacement and traction, u_i^{inc} and t_i^{inc} are displacement and traction of the incident wave.

In frequency domain, the BVP is defined by the BIE (6) and the discussed above boundary condition (2). Displacement and traction components along existing boundary Γ_I are the final result at solution of this BVP in frequency domain.

The solution of the system of BIE (6) follows a standard procedure in which all the boundaries are discretized by quadratic boundary elements. The BIE are written in a discrete form for each collocation or nodal point of the model and as a result the matrix equation system with respect to the total field quantities $\mathbf{Gt} - \mathbf{Gt}^{\text{inc}} - \mathbf{Hu} + \mathbf{Hu}^{\text{inc}} = \mathbf{0}$ is obtained, where the respective free term due the incident waves is $-\mathbf{Gt}^{\text{inc}} + \mathbf{Hu}^{\text{inc}}$. Each influence matrix component results from numerical integration of integrals containing the products of fundamental solutions times shape functions used for the field variables. All singularities in the kernels related with the boundary integral equations (6) are overcome following the detailed descriptions in Garcia-Sanchez [15]. When the static fundamental solutions, as a part of

the dynamic ones, are calculated over an element containing the collocation point the displacement-based kernels exhibit a weak singularity of $O(\ln r)$, while the traction-based kernels exhibit a strong singularity of $O(1/r)$. The integrals with weak singularity are computed using appropriate quadrature rules, while the strongly singular ones are evaluated by the rigid body motion concept. All regular parts of the integrals are calculated by using numerical integration and standard Gaussian quadrature.

Incident wave motion corresponding to horizontally propagating P- or SV-waves through the orthotropic plane in the absence of heterogeneities results in the following displacement field at a point $\mathbf{x} = (x_1, x_2)$ (see [5, 15]):

$$
\begin{aligned}
u_1^{inc}(\mathbf{x},\omega) &= u_0(-ik_{\mathrm{P}})\, e^{-ik_{\mathrm{P}}x_1} \quad \text{— incident P-wave case;} \\
u_2^{inc}(\mathbf{x},\omega) &= u_0(-ik_{\mathrm{SV}})\, e^{-ik_{\mathrm{SV}}x_1} \quad \text{— incident SV-wave case.}
\end{aligned} \tag{7}
$$

In the above, u_0 is the unit displacement amplitude of the wave, $k_{\mathrm{P}} = \omega/V_{\mathrm{P}}$ and $k_{\mathrm{SV}} = \omega/V_{\mathrm{SV}}$ are the P- and SV-wave numbers, respectively, while the corresponding phase velocities are $V_{\mathrm{P}} = \sqrt{c_{22}/\rho}$ and $V_{\mathrm{SV}} = \sqrt{c_{66}/\rho}$. Finally, following Garcia-Sanchez [15], the corresponding tractions at observation point $\mathbf{x}$ are: $t_i^{\mathrm{inc}}(\mathbf{x},\omega) = \sigma_{ij}^{\mathrm{inc}} n_j$, where n_j is the outward unit normal vector to the surface, index $i = 1,\ 2$ and stresses $\sigma_{ij}^{\mathrm{inc}}$ are:

$$
\begin{pmatrix} \sigma_{11}^{\mathrm{inc}} \\ \sigma_{22}^{\mathrm{inc}} \\ \sigma_{12}^{\mathrm{inc}} \end{pmatrix} = \begin{pmatrix} c_{11} & c_{12} & 0 \\ c_{12} & c_{22} & 0 \\ 0 & 0 & c_{66} \end{pmatrix} \begin{pmatrix} u_{1,1}^{\mathrm{inc}} \\ u_{2,2}^{\mathrm{inc}} \\ u_{1,2}^{\mathrm{inc}} + u_{2,1}^{\mathrm{inc}} \end{pmatrix} . \tag{8}
$$

Once the displacements along the interface boundaries Γ_I have been obtained, displacements and stresses at any observer point $\mathbf{x} \notin \Gamma_I$ in the anisotropic infinite plane can be recovered from the following integral representation:

$$
u_i(\mathbf{x},\omega) = \int_{\Gamma_I} U_{ij}^*(\mathbf{x},\xi,\omega) t_j(\xi,\omega)\, d\xi - \int_{\Gamma_I} T_{ij}^*(\mathbf{x},\xi,\omega) u_j(\xi,\omega)\, d\xi, \tag{9}
$$

$$
\sigma_{ij}(\mathbf{x},\omega) = c_{ijmp} u_{m,p}(\mathbf{x},\omega) \ . \tag{10}
$$

The methodology described above together with the application of inverse FFT give as a final result the frequency and time-dependent displacements, stresses and tractions at any point $\mathbf{x}$ of the elastic anisotropic plane containing multiple anisotropic nanoinclusions and subjected to incident elastic waves.

3 Numerical Scheme Verification

The numerical scheme for solution of the boundary-value problem defined in Section 2 by the BIEM, using the fundamental solution for the continuum of general

anisotropy is based on discretization and collocation technique. The good convergence in numerical solution is achieved when the well-known accuracy condition is satisfied: $\lambda_{\text{SV}} = 10l_{\text{BE}}$, where λ_{SV} is the wave-length of the shear wave and l_{BE} is the length of the boundary element. After discretization, collocation and boundary condition satisfaction a system of linear algebraic equations is obtained with respect to the unknown displacements and tractions along the boundaryΓ_I. The described numerical scheme is for solution in frequency domain. The solutions in time-domain are obtained by the usage of direct and inverse FFT technique. A source code has been developed using Matlab software [16] and in order to verify its accuracy, some test examples are solved and the results are compared against available in the literature results.

To the authors' best knowledge, there are no results in the literature for nonuniform dynamic stress-strain state in the case of in-plane wave motion in a generally anisotropic infinite plane containing multiple anisotropic nanoinclusions. Due to this reason the verification study is based on the available results for elastic isotropic materials at nanoscale and for elastic anisotropic case without taking into account the surface elasticity properties.

Test example 1: *A nanoscale circular inclusion in an infinite plate under incident P-and SV- waves. Comparison with available in the literature solutions.*

As a first benchmark example is considered an infinitely extending, elastic isotropic matrix with prescribed bulk elastic Lame moduli λ_M, μ_M and density ρ_M, which contains a circular elastic isotropic nanoinclusion of radius a, elastic properties λ_I, μ_I and density ρ_I. The interface surface elastic characteristics are μ^S, ρ^S and $\tau^0 = 0$. The dynamic excitation comes from an incident longitudinal P- or shear SV-wave with frequency ω propagating along the $0x_1$ axis, see Fig. 2.

This benchmark example was solved by Ru et al. [6] using the semi-analytical wave function expansion method. A dimensionless parameter is now introduced that captures interface effects at the nanoscale, which is defined as $s = (2\mu^S + \lambda^S)/2\mu_M a$. This parameter becomes noticeable only at the nanoscale and controls the solution of elastodynamic problems for heterogeneous media at that scale. All presented results in the current paper are obtained by the BIEM based on the fundamental solution for anisotropic material. The case of isotropic material is treated just by setting $c_{11} = c_{22} = \lambda + 2\mu$ and $c_{12} = \lambda$, $c_{66} = \mu$.

The first set of comparison between our results obtained by the BIEM based on the anisotropic fundamental solution (reduced to the case of isotropic elasticity) and those in Ru et al. [6] for elastic isotropic material is summarized in Fig. 3. The horizontally propagating P-wave is under consideration. More specifically, the dynamic stress concentration factor (DSCF) is depicted at points along the interface

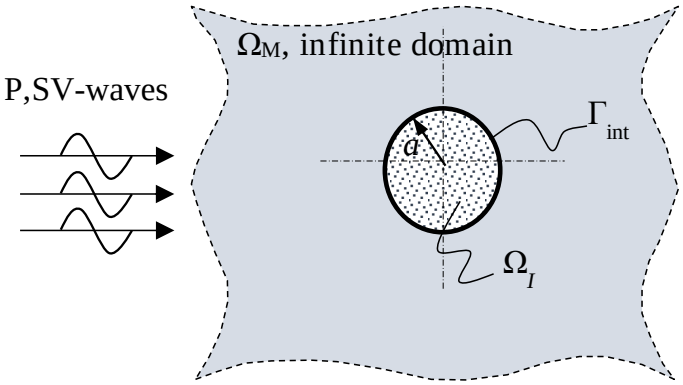

Fig. 2: Problem geometry.

perimeter from the matrix side. It is defined as $\text{DSCF}_S = |\sigma_{\varphi\varphi}/\sigma_0|$, where S is the interface perimeter from the matrix side. The obtained solutions are for a fixed non-dimensional frequency $\Omega_M = k_{P,M}a$ for P-wave, where the corresponding wave number is $k_{P,M} = \omega/C_{P,M}$ and phase velocity is $C_{P,M} = \sqrt{(\lambda_M + 2\mu_M)/\rho_M}$. We note that the DSCF is normalized by the incident stress defined as $\sigma_0 = -\mu_M u_0(\omega/C_{SV,M})^2$, where u_0 is the unit amplitude of the incident wave, $C_{SV,M}$ is the shear wave velocity of the elastic matrix. All results in Fig. 3 are plotted for fixed values of the stiffness ratio $\mu_I/\mu_M = 0.2$, which corresponds to the fixed frequency ratio $\Omega_I/\Omega_M = 3.0$. Poisson's ratio for both matrix and inclusion materials is $\nu = 0.26$, while different

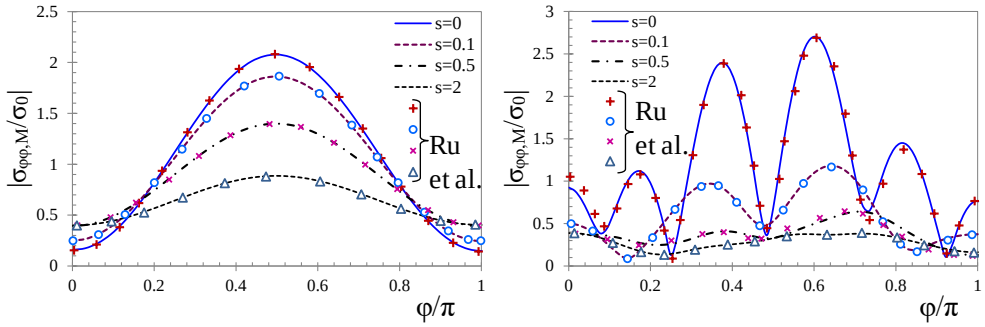

Fig. 3: DSCF along the perimeter of a circular elastic isotropic nanoinclusion from the elastic isotropic matrix side (φ is the polar angle) at fixed different values of the surface elastic parameter s and at fixed normalized frequencies of the horizontal incident P-wave: (a) Ω_M =0.2; (b) $\Omega_M = \pi$. Comparison is with results in Ru et al. [6].

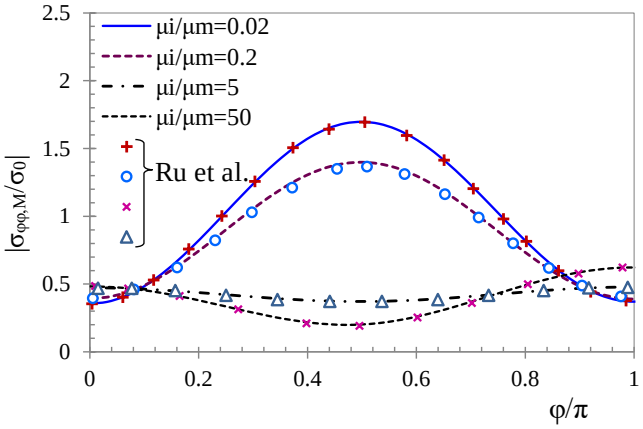

Fig. 4: DSCF along the perimeter of a circular elastic isotropic nanoinclusion from elastic isotropic matrix side at variable shear modulus ratio μ_I/μ_M and at fixed normalized frequency $\Omega_M = 0.2$ of the horizontal incident P-wave. Comparison is with results in Ru et al. [6].

values of the surface parameter $s = 0$; 0.1; 0.5; 2.0 are considered. Figures 3a, b are plots for $\Omega_M = 0.2$ and $\Omega_M = \pi$, respectively. Excellent agreement is observed between these two sets of results obtained by two very different computational techniques. Finally, our BIEM implementation employed a mesh comprising 32 quadratic boundary elements for the low frequency case of $\Omega_M = 0.2$ and 64 quadratic boundary elements for the higher frequency $\Omega_M = \pi$.

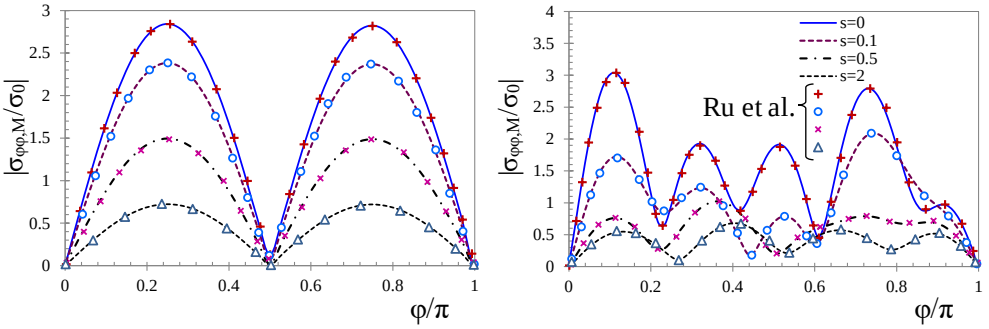

Fig. 5: DSCF along the perimeter of a circular elastic isotropic nanoinclusion from elastic isotropic matrix side at variable values of the surface elastic parameter s and at fixed normalized frequencies of incident SV-wave: (a) $\Omega_M = 0.2$; (b) $\Omega_M = \pi$. Comparison is with results in Ru et al. [6].

Figure 4 compares the DSCF induced by P-wave with normalized frequency $\Omega_M = 0.2$ for various ratios of shear modulus μ_I/μ_M, starting by softer inclusion with $\mu_I/\mu_M = 0.02$ and reaching the stiffer inclusion case with $\mu_I/\mu_M = 50$. Again the comparison is with respect to the results reported by Ru et al. [6]. In all the plots portrayed in Fig. 4, the surface elasticity parameter $s = 0.5$, the frequency ratio of softer to stiffer phase is set to $\Omega_{\text{softer}}/\Omega_{\text{stiffer}} = 3.0$.

The DSCF induced by incident SV-wave propagating along the axis $0x_1$ is illustrated in Fig. 5. Here the frequency is normalized with respect to the phase velocity of the shear SV-wave, i.e. $\Omega_M = k_{\text{SV},M}a$, where the corresponding wave number is $k_{\text{SV},M} = \omega/C_{\text{SV},M}$ and shear phase velocity is $C_{\text{SV},M} = \sqrt{\mu_M/\rho_M}$. As before different values of the surface parameter are set in the simulations and comparisons with the results presented in Ru et al. [6] have been done.

Test example 2: *A circular elastic anisotropic inclusion in an infinite elastic anisotropic plate under incident P-wave and interface pressure. Comparisons with FEM.*

The second test example is a circular elastic anisotropic inclusion of radius a in an infinite anisotropic plate. The idea of comparison with FEM is to fix the discretization mesh in the frequency and time intervals under consideration and proves the accuracy of the developed BEM codes. Two types of loading are considered: (a) far field static load that is equivalent to a longitudinal P-wave stress field, i.e., $t_1 = \sigma_0$; $t_2 = \sigma_0\nu/(1-\nu)$, and (b) an interface pressure of intensity p acting on the contact inclusion-matrix interface, see Fig. 6. There is a lack of results concerning anisotropic inclusion embedded in an anisotropic infinite plate. That is the reason why we compare our solutions with the FEM solutions obtained by the authors and ANSYS software [17]. In the finite element model the square plate of size $500a$ has been modeled with a circular inclusion of radius a in its center.

The anisotropic infinite plate is made of LiNaKCsPO3 Glass Fiber. Material stiffness tensor components are: $c_{11} = 193.946$ MPa; $c_{12} = 17.952$ MPa; $c_{22} = 39.313$ MPa; $c_{66} = 13$ MPa, density is $\rho = 2.8$ t/m^3, the radius of the inclusion is $a = 10^{-9}$ m.

The inclusion material is assumed 10 times softer, or the respective stiffness tensor is $c_{11,I} = 19.3946$ MPa; $c_{12,I} = 1.7952$ MPa; $c_{22,I} = 3.9313$ MPa; $c_{66,I} = 1.3$ MPa, with inclusion's density 1 t/m^3. An equivalent isotropic matrix material with Lame constants $\lambda = c_{12} = 17.952$ MPa and $\mu = c_{66} = 13$ MPa corresponding to the anisotropic one is considered with the respective 10 times softer inclusion. The BEM comprises of 32 quadratic boundary elements for the inclusion-matrix interface. The FE mesh comprises of 43286 8-noded plane strain FE (PLANE183). 200 FE are located along the inclusion-matrix interface and 100 FE are used per each side of

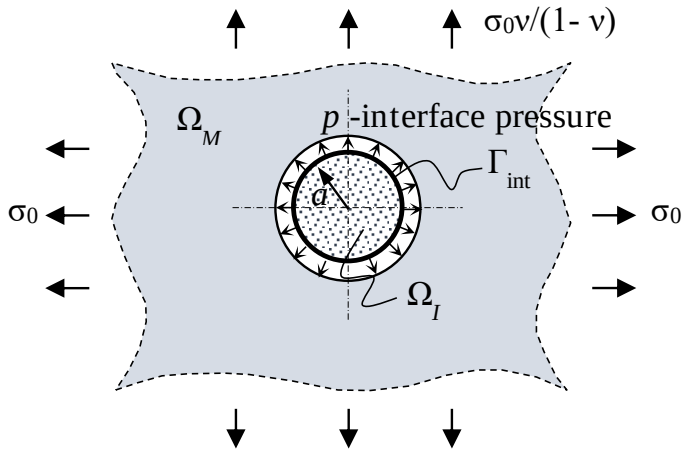

Fig. 6: Circular elastic anisotropic inclusion in an infinite elastic anisotropic plate – geometry and loading

the plate. The time harmonic analysis is performed for frequency range up to $\Omega = \omega a/\sqrt{c_{66,M}/\rho_M} = 6$ divided into 50 equal frequency steps. Constant hysteretic material damping is assigned equal to 5%.

The first set of comparisons concerning elastic isotropic matrix and inclusion and surface pressure loading case are presented in Fig. 7. More specifically, the normalized horizontal displacements $u_1 c_{66,M}/ap$ and $u_2 c_{66,M}/ap$ for points of the nanoinclusion-matrix interface with polar angle φ =0 and $\varphi = \pi/2$ respectively ver-

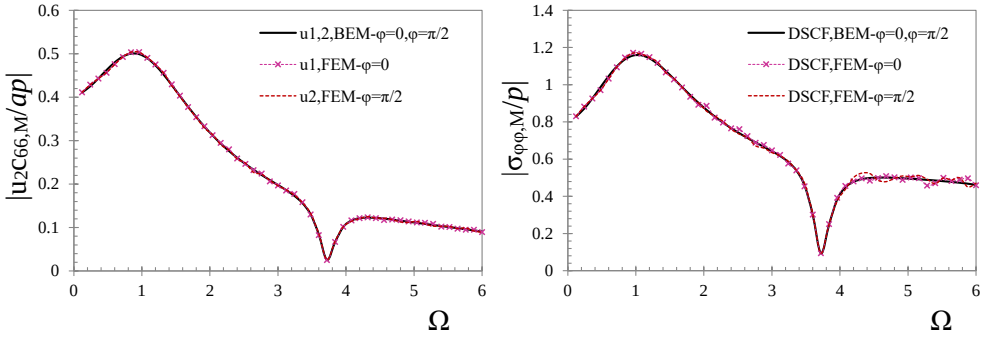

Fig. 7: Circular elastic isotropic inclusion in an infinite elastic isotropic plate: a) normalized displacement components; b) DSCF. Comparison between BIEM and FEM.

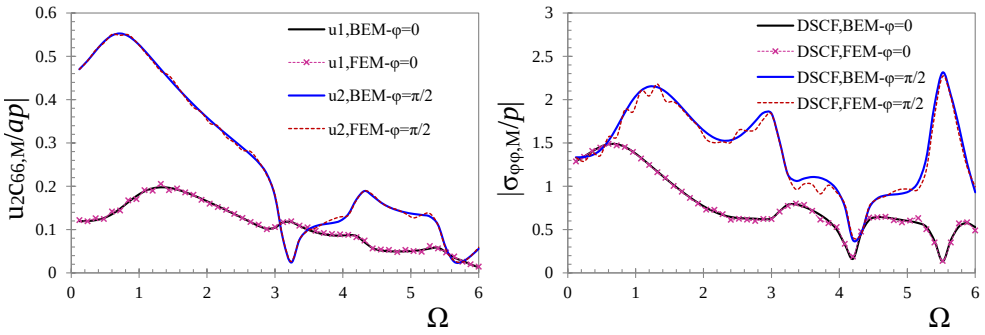

Fig. 8: Circular elastic anisotropic inclusion in an infinite anisotropic plate: a) normalized displacement components; b) DSCF. Comparison between BIEM and FEM.

sus normalized frequency $\Omega = \omega a/\sqrt{c_{66,M}/\rho_M}$ are portrayed in Fig. 7a. The DSCF defined as $|\sigma_{\varphi\varphi}/p|$ for the same observer points is compared in Fig. 7b. The same set of results for the anisotropic matrix and inclusion in case of surface pressure loading is portrayed in Fig. 8.

The case of far field static load equivalent to a longitudinal P-wave is compared in Table 1. The static solution of the BIEM is obtained by elastodynamic fundamental solution for anisotropic material and low dimensionless frequency value of $\Omega_M = 0.001$. The matrix material is always isotropic as far as the equivalent static load is applicable for isotropic one. The inclusion is isotropic and anisotropic in both the FEM and BEM models. The percentage differences between BEM and FEM solutions are calculated with respect to the average values.

The verification study results show that the type of discretization is sufficient to achieve a satisfactory accuracy in our parametric study. The results shown in all figures above illustrate clearly that the developed numerical scheme and the created software work with a high accuracy and we can continue further with the simulation study, which is presented in Part II of the current work.

Table 1: Comparison between BEM and FEM in case of static solution

	FEM		BEM		Percentage difference	
	$\sigma_{\varphi\varphi}/\sigma_0$ $\varphi = 0$	$\sigma_{\varphi\varphi}/\sigma_0$ $\varphi = \pi/2$	$\sigma_{\varphi\varphi}/\sigma_0$ $\varphi = 0$	$\sigma_{\varphi\varphi}/\sigma_0$ $\varphi = \pi/2$	$\varphi = 0$	$\varphi = \pi/2$
Iso incl	0.246429	2.18572	0.245856	2.18706	0.23	0.06
Aniso incl	0.703441	1.31312	0.70333	1.31677	0.02	0.28

4 CONCLUSIONS

This Part I presents mechanical model and computational methodology for solution of 2D elastodynamic problem considering an infinite anisotropic plane with multiple anisotropic nanoinclusions of arbitrary geometry, number and mutual disposition. The mechanical model is based on a combination of surface elasticity theory with the BEM, taking into account the material anisotropy. The proposed mechanical model is used as a base in an accompanied paper (Part II) for a parametric study revealing different phenomena in the scattered wave fields due to the influence of anisotropy and surface elasticity.

ACKNOWLEDGMENT

The first author wishes to acknowledge support provided by the Research, Consultancy and Design Centre (RCDC) of UACEG-Sofia through Grant No БН-298/24. The second author is supported by the Bulgarian National Science Fund, contract No КП-06-Н57/3/15.11.2021.

REFERENCES

[1] M.E. GURTIN, A.I. MURDOCH (1975) A continuum theory of elastic material surfaces. *Archive for Rational Mechanics and Analysis* **57** 291-323.

[2] G. MANOLIS, P. DINEVA, T. RANGELOV, D. SFYRIS (2021) Mechanical Models and Numerical Simulations in Nanomechanics: A review across the scales. *Engineering Analysis with Boundary Elements* (*EABE)* **128** 149-170.

[3] T. PETROVA (2023) Analytical modeling of stresses and strains for nanocomposite structures - opportunities and challenges. *Bulgarian Chemical Communications* **55**(3) 349-366.

[4] Y.H. PAO, C.-C. MOW (1973) "Diffraction of Elastic waves in Dynamic Stress Concentrations" Crane-Russak, New York.

[5] J. DOMINGUEZ (1993) "Boundary Elements in Dynamics" Computational Mechanics Publications, Southampton.

[6] Y. RU, G.F. WANG, T.J. WANG (2009) Diffraction of elastic waves and stress concentration near a cylindrical nano-inclusion incorporating surface effect. *Journal of Vibration and Acoustics* **131** (6) 061011-1-061011-7.

[7] Q.F. ZHANG, G.F. WANG, P. SCHIAVONE (2011) Diffraction of plane compressional waves by an array of nanosized cylindrical holes. *Journal of Applied Mechanics, Transactions ASME* **78**(2) 021003 (6 pages).

[8] Z.S. OU, D.W. LEE (2012) Effects of Interface Energy on Scattering of Plane ElasticWave by a Nano-Sized Coated Fiber. *Journal of Sound and Vibration* **33** 5623-5643.

[9] S. PARVANOVA, G. MANOLIS, P. DINEVA (2015) Wave scattering by nanoheterogeneities embedded in an elastic matrix via BEM. *Engineering Analysis with Boundary Elements* **56** 57-69.

[10] S. PARVANOVA, G. VASILEV, P. DINEVA, G. MANOLIS (2016) Dynamic analysis of nano-heterogeneities in a finite-sized solid by boundary and finite element methods. *International Journal of Solids and Structures* **80** 1-18.

[11] S. SODAGAR, A. GURAN (2012) Interaction of Elastic Waves with a Cylindrical Nano-Inclusion. *AIP Conference Proceedings* **1487** 248-255.

[12] L. TIAN, R.K.N.D. RAJAPAKSE (2007) Elastic field of an isotropic matrix with a nanoscale elliptical inhomogeneity. *International Journal of Solids and Structures* **44** 7988-8005.

[13] C.Y. WANG, J.D. ACHENBACH (1994) Elastodynamic fundamental solutions for anisotropic solids. *Geophysical Journal International* **118** 384-392.

[14] P. DINEVA, T. RANGELOV, D. GROSS (2005) BIEM for 2D steady-state problems in cracked anisotropic materials. *Engineering Analysis with Boundary Elements* **29** 689-698.

[15] F.G. GARCIA-SANCHEZ (2005) "Numerical study of fracture problems in elastic anisotropic and piezoelectric solids" Dissertation, University of Sevilla, Spain.

[16] MATLAB version 8.2.0.701 (R2013b). The MathWorks Inc, Natick, Massachusetts, 2013.

[17] ANSYS 2011. Release 14.0, Structural Mechanics Package. Canonsburg, Pennsylvania